www.czasopisma.pan.pl PAN POLSKA AKADEMIA NAUK www.journals.pan.pl

Arch. Metall. Mater. **69** (2024), 1, 39-43

DOI: https://doi.org/10.24425/amm.2024.147781

SEUNG-HYEOK SHIN[1], DONG-KYU OH[1], SANG-GYU KIM[1], BYOUNGCHUL HWANG[1*]

EFFECT OF MICROSTRUCTURAL CONSTITUENTS ON HYDROGEN EMBRITTLEMENT RESISTANCE OF API X60, X70, AND X80 PIPELINE STEELS

This study describes how microstructural constituents affected the hydrogen embrittlement resistance of high-strength pipeline steels. The American Petroleum Institute (API) X60, X70, and X80 pipeline steels demonstrated complicated microstructure comprising polygonal ferrite (PF), acicular ferrite, granular bainite (GB), bainitic ferrite (BF), and secondary phases, e.g., the martensite-austenite (MA) constituent, and the volume fraction of the microstructures was dependent on alloying elements and processing conditions. To evaluate the hydrogen embrittlement resistance, a slow strain rate test (SSRT) was performed after electrochemical hydrogen charging. The SSRT results indicated that the X80 steel with the highest volume fraction of the MA constituent demonstrated relatively high yield strength but exhibited the lowest hydrogen embrittlement resistance because the MA constituent acted as a reversible hydrogen trap site.

Keywords: Pipeline steel; microstructure; hydrogen embrittlement; electrochemical hydrogen charging; slow strain rate test (SSRT)

1. Introduction

In recent years, as environmental problems caused by CO_2 emissions from fossil fuels have become severe, hydrogen energy is garnering attention as a next-generation energy [1-6]. Considering that the American Petroleum Institute (API) pipeline steels used to transport natural gas are frequently exposed to high-pressure hydrogen environments, hydrogen embrittlement may occur, which deteriorates the mechanical properties of materials [7-9]. It has been reported that an increase in the strength level deteriorates the hydrogen embrittlement resistance [10,11]. However, it is challenging to understand the effect of each microstructural constituent on the hydrogen embrittlement resistance of pipeline steels owing to their very complicated microstructures [12-16]. Thus, it is necessary to investigate the correlation between characterized microstructural constituents and the hydrogen embrittlement resistance to develop API pipeline steels possessing an excellent combination of strength and hydrogen embrittlement resistance.

In the present study, the API X60, X70, and X80 pipeline steels with different microstructural constituents were fabricated by varying alloying elements and thermomechanical control processing conditions. The slow strain rate test (SSRT) and silver decoration were performed after electrochemical hydrogen charging to investigate the hydrogen embrittlement resistance.

2. Experimental

Three pipeline steels fabricated in this study are API X60, X70, and X80 grade steels having above the yield strength levels of 413 MPa (60 psi), 483 MPa (70 psi), and 552 MPa (80 psi), respectively. The chemical compositions, processing conditions, and specific transformation temperatures of investigated steels are summarized in TABLE 1 [17-20].

The microstructures of the X60, X70, and X80 steels were observed using an FE-SEM (JSM-6700F, JEOL, Japan) after mechanically polishing and etching with a 3% Nital solution. Secondary phases, e.g., the martensite-austenite (MA), were detected using the LePera etching method [21], and the volume fraction of the MA was measured using an image analyzer (Image-Pro Plus 10, Media Cybernetics Inc., USA). The specimens for the EBSD analysis (EDAX-TSL, Digiview-IV, USA) were mechanically polished and then electro-polished in a mixed solution of 90% glacial acetic acid (CH_3COOH) and 10% perchloric acid ($HClO_4$). The acceleration voltage, working distance, and step size considered for EBSD analysis were 15 kV, 12 mm, and 0.18 μm, respectively. The EBSD data were obtained from the Orientation Imaging Microscopy (OIM) Analysis™ (TexSEM Laboratories, USA)

Sub-size round tensile specimens (ASTM E8 standard) with a gauge diameter of 6.3 mm and a gauge length of 25.4 mm were

[1] SEOUL NATIONAL UNIVERSITY OF SCIENCE AND TECHNOLOGY, DEPARTMENT OF MATERIALS SCIENCE AND ENGINEERING, 232 GONGNEUNG-RO, NOWON-GU, SEOUL 01811, REPUBLIC OF KOREA

* Corresponding author: bhwang@seoultech.ac.kr

machined from the plate along the rolling direction. The tensile test was performed with a slow strain rate of 5.0×10^{-5} s^{-1} at room temperature using a universal testing machine with a capacity of 10 tons (UT-100E, MTDI, Korea). To simulate pipe forming and coating processes, the specimens were additionally pre-strained to 5%. Stress corresponding to 0.5% strain was determined to be the yield strength of the API pipeline steels [22]. Some tensile specimens were electrochemically hydrogen-charged in an aqueous solution of 3 wt.% NaCl and 0.3 wt.% NH_4SCN with a current density of 150 Am^{-2} for 24 hours using a Pt wire as a counter electrode. The specimen before charging was marked as Non-charged, and the specimen after charging was referred to as H-charged. After the SSRT, fractured tensile specimens were observed using an SEM (EVO10, Carl Zeiss, Germany). For a comparative evaluation of hydrogen embrittlement resistance, the relative total elongation was calculated using the following equation:

$$Relative\,total\,elongation = \frac{Total\,elongation_{H-charged}}{Total\,elongatoin_{Non-charged}}$$

To perform silver decoration, the X80 steel was electrochemically hydrogen-charged in a mixed aqueous solution of 3 wt.% NaCl and 0.3 wt.% NH_4SCN with a current density of 150 Am^{-2} for 24 hours. After hydrogen charging, the specimen was maintained in a 4.3 mM $K[Ag(CN)_2]$ solution for 24 hours. Silver clusters precipitated by the reaction of hydrogen and silver ions adsorbed on the surface of the specimens were examined using an SEM.

3. Results and discussion

Fig. 1 shows the SEM and OM micrographs of the three API pipeline steels. Based on morphology and transformation behavior, the microstructures of API pipeline steels fabricated by the thermomechanical control process can be classified [23-25]. As shown in Fig. 1(a), the API X60, X70, and X80 steels have various microstructures of polygonal ferrite (PF), acicular ferrite (AF), granular bainite (GB), and bainitic ferrite (BF). After LePera etching to confirm the MA, the ferrite and bainitic micro-

TABLE 1

Chemical composition (wt.%) thermomechanical processing conditions, and specific transformation temperatures of the API X60, X70, and X80 pipeline steels [17-20]

Steel	* Chemical composition (wt.%)			Thermomechanical processing conditions				Transformation temperature		
	C	Si	Mn	Strat rolling temperature ℃	Finish rolling temperature ℃	Strat cooling temperature ℃	Cooling rate ℃/s	Non-recrystallization temperature ℃	Bainite start temperature ℃	Martensite start temperature ℃
X60	<0.06	0.25	<1.50	>1,050	>950	>800	>30	965	630	475
X70	<0.07	0.25	<1.70	>950	>880	>780	>20	974	625	476
X80	<0.08	0.24	<1.80	<950	<800	>750	<20	1,068	609	454

* The API X60, X70, and X80 pipeline steels contain from 0.1 to 0.5 (Ni+Cr+Mo) and from 0.05 to 0.2 (Nb+Ti+V) (wt %).
* To improve the hardenability, Cu and B are added to the API X80 pipeline steel.

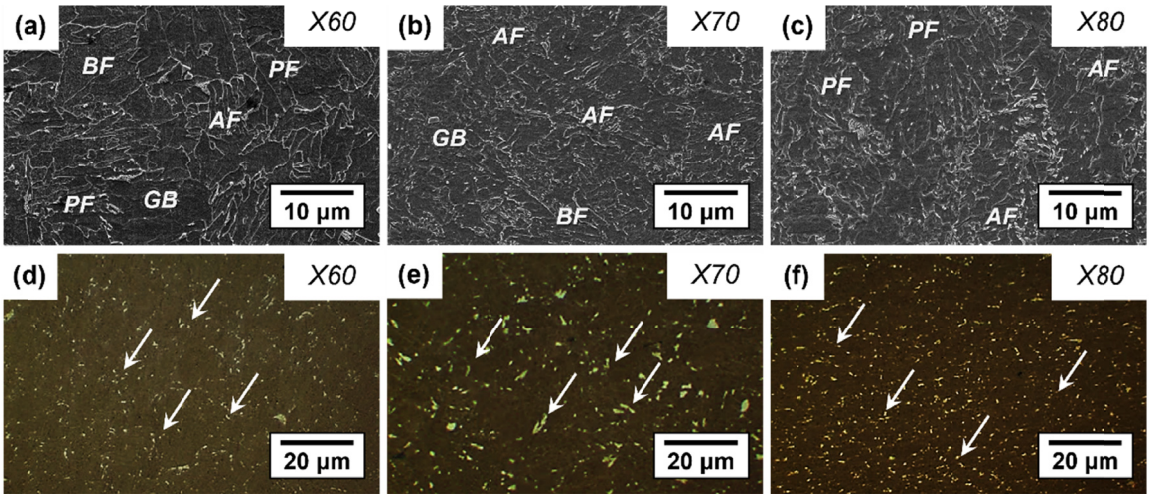

Fig. 1. (a-c) Scanning electron microscope (SEM) micrographs and (d-f) optical micrographs of microstructures of the API X60, X70, and X80 pipeline steels, respectively [11]. Longitudinal-transverse (L-S) planes are observed. Polygonal ferrite (PF), acicular ferrite (AF), granular bainite (GB), and bainitic ferrite (BF) are marked in Figs. 1(a-c). Figs. 1(d-f) show the microstructure etched in Lepera solution, and martensite-austenite (MA) constituents are indicated by the white arrow. The volume fraction of the MA constituent in the API X60, X70, and X80 pipeline steels was measured to be 4.3%, 6.0%, and 7.8%, respectively

structures have exhibited brown color, and the MA constituent has illustrated white color (Fig. 1(b)). Despite the slowest cooling rate, the X80 steel demonstrated the highest volume fraction of the MA, as its hardenability was significantly enhanced owing to the highest carbon (C) content and the addition of boron (B) and copper (Cu) [13].

For detailed microstructure characterization, an EBSD analysis was conducted. Fig. 2 exhibits the EBSD inverse pole figure (IPF) and grain boundary misorientation maps of the X60, X70, and X80 steels. In the IPF maps, each microstructure is indicated by various colors corresponding to the crystal orientation of each point. The PF and AF have exhibited fine grain size, and the GB and BF have revealed coarse grains with many sub-grain boundaries and MA. The X80 steel has exhibited the finest grain size of 16.1 μm, whereas the X60 steel has demonstrated a large grain size of 20.5 μm. Owing to a decrease in the rolling start and end temperatures, the volume fractions of PF and AF increased, and the grain size decreased. Previous studies [26,27] reported that PF and AF had fine grains with high-angle grain boundaries (HAGBs, >15°), whereas GB and BF exhibited relatively coarse grains with high fractions of the low-angle grain boundaries (LAGBs, 5° ~ 15°). Regarding the fraction of the misorientation

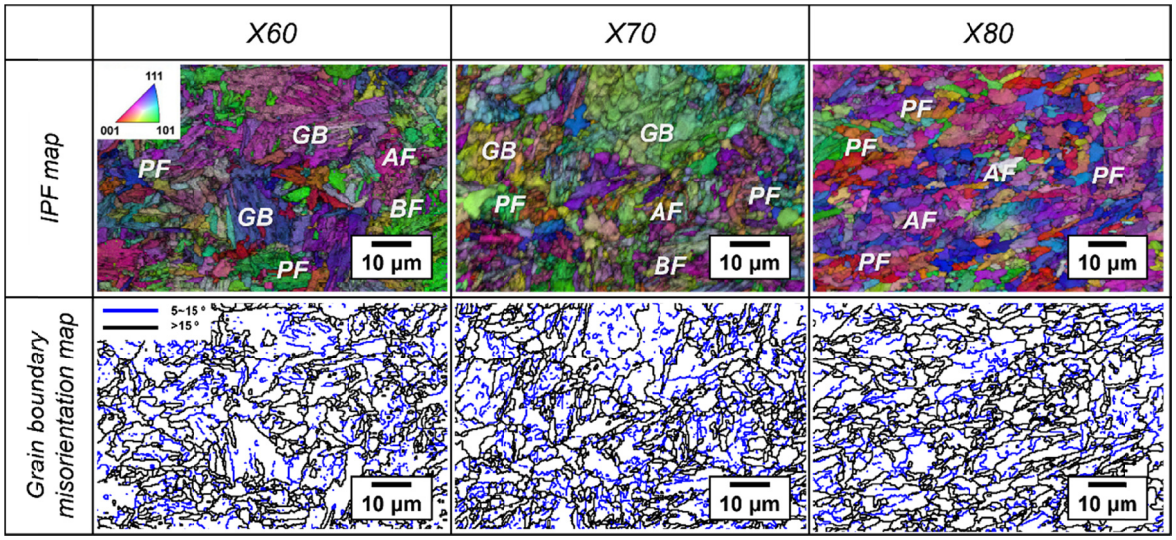

Fig. 2. Electron backscatter diffraction (EBSD) inverse pole figure (IPF) and grain boundary misorientation maps of the API X60, X70, and X80 pipeline steels [11]. Longitudinal-transverse (L-S) planes are observed. Polygonal ferrite (PF), acicular ferrite (AF), granular bainite (GB), and bainitic ferrite (BF) are marked in IPF maps. In grain boundary misorientation maps, the angle ranges of blue and black lines are 5 ~ 15°, and >15°, respectively. The grain size and fraction of the high-angle grain boundary of the API X60, X70, and X80 pipeline steels were calculated to be 20.5 μm and 4.3%, 17.6 μm and 6.0%, and 16.1 μm and 7.8%, respectively

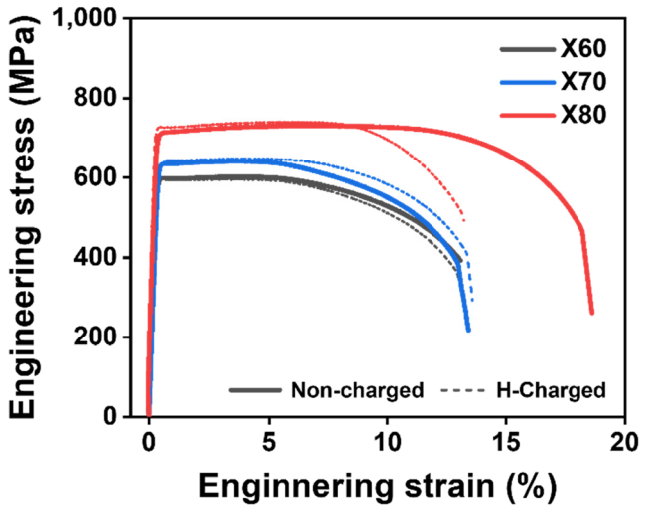

Fig. 3. Engineering stress-strain curves before and after electrochemical hydrogen charging of the API X60, X70, and X80 pipeline steels. The specimen before electrochemical hydrogen charging was marked as Non-charged, and the specimen after electrochemical hydrogen charging was referred to as H-charged. The relative total elongation of the API X60, X70, and X80 pipeline steels was measured to be 0.99, 1.02, and 0.72, respectively

angle in the grain boundary misorientation maps, the X60 steel reveals a relatively high fraction of the LAGB because it was rolled in the austenitic recrystallization region and rapidly cooled, resulting in high fractions of GB and BF. However, the X80 steel fabricated at the lowest finish rolling temperature and the slowest cooling rate reveals the highest fraction of the HAGB because many prior austenite grain boundaries and deformed austenite bands act as nucleation sites for PF and AF.

The engineering stress-strain curves of the H-charged and non-charged specimens of the X60, X70, and X80 steels are provided in Fig. 3. The H-charged and non-charged specimens of all the steels exhibit continuous yielding behavior, and the yield strength is higher than the strength requirements of the API specification (X60: 413 MPa, X70: 483 MPa, and X80: 552 MPa) due to pre-strain. The X60 steel having relatively coarse grains and a low volume fraction of the MA exhibits the lowest yield strength of 597 MPa, whereas the X80 steel has the highest yield strength of 710 MPa because of the highest volume fraction of the MA and fine grains. However, the H-charged X80 steel specimen reveals the lowest hydrogen embrittlement resistance with a relative total elongation of 0.72.

The silver decoration was performed after electrochemical hydrogen charging to examine the low hydrogen embrittlement resistance of the X80 steel. As shown in Fig. 4, the distribution of silver clusters in PF, AF, GB, and BF makes it difficult to differentiate, however, several small and large silver clusters are localized around the MA. For the tensile fractured surfaces (Fig. 5), the non-charged specimens of the X60, X70, and X80 steels exhibit ductile fracture behaviors including many dimples, whereas the H-charged specimen of the X80 steel reveals brittle fracture behaviors, indicating some quasi-cleavage fracture surfaces. Based on these results, it can be implied that the MA formed by enhanced hardenability acts as a reversible hydrogen trap site to mobilize diffusible hydrogen, thereby decreasing the hydrogen embrittlement resistance of the X80 steel.

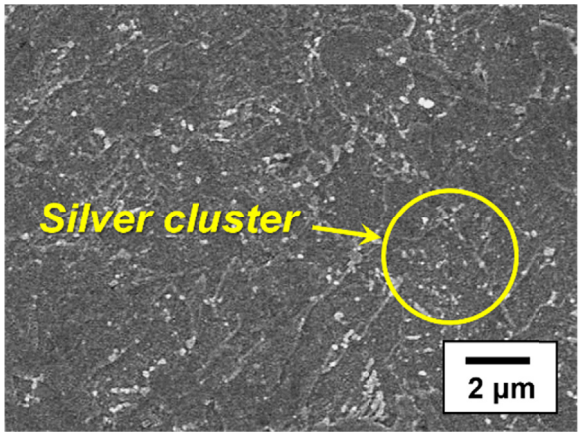

Fig. 4. Scanning electron microscope (SEM) micrograph of the API X80 pipeline steel after electrochemical hydrogen charging for 24 hours at the current density of 150 A/m^2 in the 3% NaCl solution. After electrochemical hydrogen charging, the specimen was maintained in a 4.3 mM $K[Ag(CN)_2]$ solution for 24 hours. The yellow arrow in Fig. 4 shows the localized precipitation of silver clusters surrounding martensite-austenite (MA) constituents

4. Conclusions

In the present study, the correlation between the microstructure and hydrogen embrittlement resistance of three API pipeline steels fabricated by varying alloying elements and processing conditions was investigated. The following conclusions were drawn:

1) The X60, X70, and X80 steels had different grain sizes and volume fractions of PF, AF, GB, BF, and MA constituents depending on the alloying elements and processing conditions.
2) The X80 steel having the finest grain size and the highest volume fraction of the MA showed the highest yield strength regardless of electrochemical hydrogen charging but revealed the lowest hydrogen embrittlement resistance among all the steels.
3) Based on the results of silver decoration and SEM fractography after electrochemical hydrogen charging, it can be implied that the lowest hydrogen embrittlement resistance of the X80 steel was caused by a large amount of MA acting as a reversible trap site for hydrogen.

Acknowledgments

This study was supported by the Research Program funded by the SEOULTECH (Seoul National University of Science and Technology).

REFERENCES

[1] S.Y. Lee, S.I. Lee, B. Hwang, Mater. Sci. Eng. A **711**, 22-28 (2019).
[2] S.I. Lee, S.Y. Lee, B. Hwang, Mater. Sci. Eng. A **742**, 334-343 (2019).

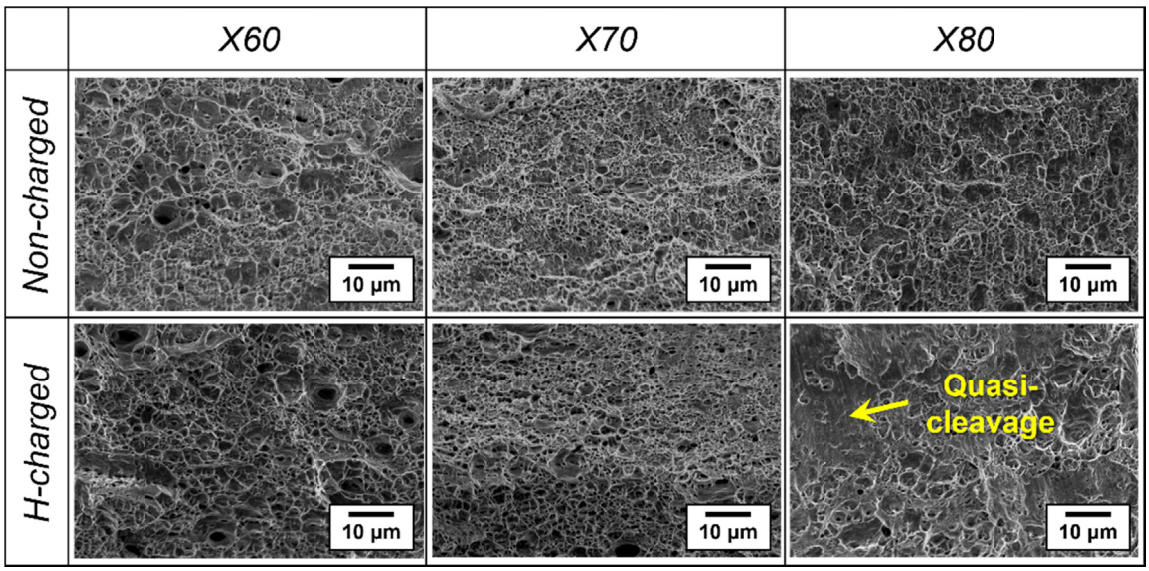

Fig. 5. Scanning electron microscope (SEM) fractographs for tensile specimens of the API X60, X70, and X80 pipeline steels before and after electrochemical hydrogen charging. The specimen before electrochemical hydrogen charging was marked as Non-charged, and the specimen after electrochemical hydrogen charging was referred to as H-charged. The yellow arrow indicates the quasi-cleavage fracture features in the API X80 pipeline steel.

[3] K.M. Ryu, D.G. Lee, J. Moon. C.H. Lee, T.H. Lee, J.S. Lee, D.W. Suh, Met. Mater. Int. **27**, 425-435 (2021).
[4] M. Asadipoor, J. Kadkhodapour, A.P. Anaraki, S.M.H. Sharifi, A.Ch. Darabi, A. Barnoush, Met. Mater. Int. **27**, 2276-2291 (2021)
[5] M. Ranjbar. R. Miresmaeili, M.R. Naimi-Jamal, M. Miraei, Met. Mater. Int. **27**, 3918-3934 (2021).
[6] E. Ma, S. Park, H. Choi, B. Hwang, J. Byun, J. Powder Mater. **30**, 217-222 (2023).
[7] S.K. Dwivedi, M. Vishwakarma, Int. J. Hydrog. **43**, 21603-21616 (2018).
[8] M. Wang, C.C. Tasan, M. Koyama, D. Ponge, D. Raabe, Metall. Mater. Trans. A **46**, 3797-3802 (2015).
[9] J.H. Ryu, Y.S. Chun, C.S. Lee, H.K.D.H. Bhadeshia, D.W. Suh, Acta Mater. **60**, 4085-4092 (2012).
[10] G. Sandoz, Met. Trans. **3** (1972) 1169.
[11] K. Farrell, A.G. Quarrel, J. Iron Steel Inst. **202** (1964) 1002.
[12] S.W. Lee, S.I. Lee, B. Hwang, Korean J. Met. Mater. **58**, 1-12 (2020).
[13] S.I. Lee, S.W. Lee, S.G. Lee, H.G. Jung, B. Hwang, Met. Mater. Int. **24**, 1221-1231 (2018).
[14] S.I. Lee, J. Lee, B. Hwang, Mater. Sci. Eng. A **758**, 56-59 (2019).
[15] H.K. Sung, D.H. Lee, S. Lee, H.S. Kim, Y. Ro, C.S. Lee, B. Hwang, S.Y. Shin, Metall. Mater. Trans. A **47**, 2726-2738 (2016).
[16] X.L. Yang, Y.B. Xu, X.D. Tan, D. Wu, Mater. Sci. Eng. A **607**, 53-62 (2014).
[17] S.Y. Han, S.Y. Shin, C.H. Seo, H. Lee, J.H. Bae, K. Kim, S. Lee, N.J. Kim, Metall. Mater. Trans. A **40**, 1851-1862 (2009).
[18] C. Capdevila, C.G. Andres, ISIJ Int. **42**, 894-902 (2002).
[19] K.W. Andrew, JISI **203**, 721-727 (1965).
[20] C.Y. Kung, J.J. Raymond, Metall. Trans. A **13**, 328-331 (1982).
[21] F.S. LePera, Metallography **12**, 263-268 (1979).
[22] API Specifications 5L, Specifications for Line Pipe, 43th edn., American Petroleum Institute, USA, 1-155, (2004).
[23] B.L. Bramfitt, J.G. Speer, Metall. Trans. A **21**, 817-829 (1990).
[24] G. Krauss, S.W. Thompson, ISIJ Int. **35**, 937-945 (1995).
[25] S.W. Thompson, D.J. Colvin, G. Krauss, Metall. Mater. Trans. A **21**, 1493-1507 (1990).
[26] S.H. Shin, D.K. Oh, Y.C. Yoon, B. Hwang, Steel. Res. Int. **220479** (2022).
[27] S.I. Lee, T.W. Hong, B. Hwang, Korean J. Mater. Res. **27**, 636-642 (2017).